Nanoscale

Point Defects at Grain Boundaries Can Create Structural Instabilities and Persistent Deep Traps in Metal Halide Perovskites

Journal:	*Nanoscale*
Manuscript ID	NR-ART-08-2024-003424.R1
Article Type:	Paper
Date Submitted by the Author:	28-Nov-2024
Complete List of Authors:	Wu, Yifan; University of Southern California, Chemistry Liu, Dongyu; HSE University, Chu, Weibin; Fudan University, Wang, Bipeng; University of Southern California, Chemical Engineering Vasenko, Andrey S.; HSE University Prezhdo, Oleg; University of Southern California, Chemistry

Point Defects at Grain Boundaries Can Create Structural Instabilities and Persistent Deep Traps in Metal Halide Perovskites

Yifan Wu,[1] Dongyu Liu,[2] Weibin Chu,[3] Bipeng Wang,[1] Andrey S. Vasenko,[2,4] Oleg V. Prezhdo[1,5*]

[1]*Department of Chemistry, University of Southern California, Los Angeles, CA 90089, USA*

[2]*HSE University, 101000 Moscow, Russia*

[3]*Key Laboratory of Computational Physical Sciences (Ministry of Education), Institute of Computational Physical Sciences, Fudan University, Shanghai 200433, China*

[4]*Donostia International Physics Center (DIPC), 20018 San Sebastián-Donostia, Euskadi, Spain*

[5]*Department of Physics and Astronomy, University of Southern California, Los Angeles, CA 90089, USA*

Abstract:

Metal halide perovskites (MHPs) have attracted strong interest for a variety of applications due to their low cost and excellent performance, attributed largely to favorable defect properties. MHPs exhibit complex dynamics of charges and ions that are coupled in unusual ways. Focusing on a combination of two common MHP defects, i.e., a grain boundary (GB) and a Pb interstitial, we develop a machine learning model of the interaction potential, and study structural and electronic dynamics on a nanosecond timescale. We demonstrate that point defects at MHP GBs can create new chemical species, such as Pb-Pb-Pb trimers, that are less likely to occur with point defects in bulk. The formed species create structural instabilities in the GB and prevent it from healing towards the pristine structure. Pb-Pb-Pb trimers produce deep trap states that can persist for hundreds of picoseconds, having a strong negative influence on charge carrier mobility and lifetime. Such stable chemical defects at MHP GBs can only be broken by chemical means, e.g., introduction of excess halide, highlighting the importance of proper defect passivation strategies. Long-lived GB structures with both deep and shallow trap states are found, rationalizing the contradictory statements in literature regarding MHP GB influence on performance.

Keywords: All-inorganic $CsPbBr_3$ perovskite, grain boundary, lead interstitial, electron-hole recombination, charge traps, machine learning force field.

1. Introduction

Metal halide perovskites (MHPs) have attracted strong attention in recent years due to their excellent properties, such as high charge carrier mobility,[1-3] long electron-hole diffusion,[4-6] intrinsic defect tolerance,[7-9] and low cost of fabrication.[10-12] These properties make MHPs a promising material for optoelectronic and photovoltaic applications.[13-19] Solar cells based on MHPs have reaches an outstanding power conversion efficiency exceeding 25%.[20, 21] The crystal structure of MHPs creates rich opportunities for material modification and optimization, and as a result, exploration of MHPs has gone into multiple directions. Many different combinations of elements or modifications to atomic configurations are being explored [18, 22-24] in order to further enhance the power conversion efficiency,[11, 25] improve stability,[23] and replace the lead due to its toxicity.[26, 27] The diversity of MHP compositions and structures give rise to an even richer space of structural defects that can have a strong influence on material's properties. The situation is complicated further by the broad range of timescales observed in the molecular dynamics (MD) of MHPs, ranging from femtosecond local vibrations to picosecond large-scale and highly anharmonic acoustic phonons, to defect migration taking nano- to milliseconds, to structural phase transitions, phase segregation, and decomposition that can extend into many days. Grain boundaries (GBs) are particularly important structures,[28] because most of the experimental techniques used to make and process MHPs, such as low-temperature thermal evaporation and solution-based processing of perovskite films,[11, 29, 30] lead to polycrystalline structures, which inevitably contain GB defects.[29, 31]

Although extensive studies of GBs in perovskites can be found in the literature,[32-35] the debate about their detrimental or benign nature is still ongoing. Some argue that GBs are harmful because they induce nonradiative electron-hole recombination channels[36] and promote charge recombination,[37, 38] as demonstrated by the influence of grain size on excited states lifetime and material efficiency.[39, 40] Others maintain that GBs play a minor role in charge and energy losses, because they create no deep trap states and only introduce shallow defects,[41, 42] arguing that electron-hole recombination happens primarily in non-GB regions.[42] Our previous studies of a common GB in the $CsPbBr_3$ perovskite have shown that transient deep trap states can appear in the GB region due to GB deformations occurring on timescales of hundreds of picoseconds.[43-45] The complex, multi-scale evolution of the geometric and electronic structure of GBs rationalize the contradictory statements found in the literature and call for further investigations on GBs in MHPs. Our previous studies focused on stoichiometric GBs.[43-45] The situation can be complicated further by point defects, which behave differently in the bulk and GB regions.[46, 47]

Thermodynamically, MHPs have low defect formation energies.[8] In bulk $CsPbBr_3$, an interstitial defect such as Pb_i, and substitutional defects such as Br_{Pb}, and $Pb_{Br,}$ can form deep trap states[48] and accelerate nonradiative recombination and efficiency loss. The polycrystalline nature of MHPs used in many applications necessitates the need to investigate the interplay of GB and point defects.

Most of the previous simulations of perovskite GBs have focused on well-ordered stoichiometric GBs based on optimized structures or few picosecond molecular dynamics (MD) trajectories, because of the computational burden of ab initio calculations.[41, 49-53] At the same time, GBs can be disordered and nonstoichiometric,[32] with point defects segregated.[54] A more thorough study of GB properties can be achieved using machine learning (ML) techniques.[55-58] In particular, ML force fields (FFs) can be constructed based on relatively small datasets generated by ab initio calculations[59] and then used to study GB properties on nanosecond timescales,[60] approaching those of charge carrier lifetimes. Nanosecond simulations can reveal slow fluctuations and evolutions of GB regions, such as backbone realignment, angle tilting, and GB sliding, and reveal important patterns in geometric and electronic structure having a significant influence on material properties.

In this work, we develop an ML FF of the $CsPbBr_3$ perovskite and employ it to investigate evolution of geometric and electronic properties in the Σ5(210) GB containing a Pb interstitial defect (Pb_i) on a nanosecond timescale. We observe three regimes in the GB evolution, having a strong influence on charge carrier properties. A fast, 10 ps GB reconstruction opens up the bandgap and leads to formation of a Pb-Pb-Pb trimer that remains stable over the subsequent 1.5 ns. For 1 ns after the initial reconstruction, the structure fluctuates, and the trimer creates a persistent but shallow electron trap. However, the trimer creates a structural instability in the GB, and prevents it from healing. After two unsuccessful attempts every 0.4 ns, the GB starts sliding on the third attempt at 1.2 ns, and the Pb-Pb-Pb trap state becomes deep for several hundred picoseconds. Such persistent deep trap can have a strong negative influence on charge carrier mobility and lifetime, and can only be eliminated by chemical passivation, e.g., with halides that can break Pb-Pb bonds. Shallow electron trap states appear and disappear in the GB regardless of the Pb_i defects. They are localized in sub-GB regions that are jammed in unfavorable configurations. Because such shallow traps frequently approach the conduction band, they are not particularly detrimental, since trapped charges can escape into the band and participate in transport. The study highlights the complexity of the structural and charge carrier dynamics in MHPs, demonstrates the need to study such dynamics

atomistically on nanosecond and longer timescales, and provides important insights into the unusual properties of MHPs.

2. Theoretical Methodology

We construct a ML FF based on the DeepMD package,[59] utilizing a deep neural network to predict the interatomic potential energy and forces, trained based on about 40,000 ab initio calculations to control the computational cost. The Vienna ab initio Simulation Package[61] is used to perform geometry optimization and ab initio MD, and to calculate densities of states (DOS) and orbital spatial distributions. The Perdew-Burke-Ernzerhof (PBE) exchange-correlation functional is used,[62] in combination with the projected-augmented wave method[63] to describe interactions between electrons and ion cores. It should be noted that spin-orbit coupling (SOC) is strong in MHPs, because they contain heavy elements. However, a rigorous calculation requires both inclusion of SOC and accurate treatment of electronic exchange via either hybrid functionals or GW theory. Such calculations are computationally expensive. Fortunately, efficient functionals, such as PBE, exhibit cancelation of errors associated with lack of SOC and approximate treatment of electronic exchange, and provide reasonable values of energy gaps and defect levels.[64] PBE is known to produce reliable geometries, and therefore, it is well suited for generating the ML FF. Van der Waals interactions play an important role in determining structural and electronic properties of MHPs, including point defects.[65] The van der Waals interactions are described by the D3 method of Grimme.[66] The plane-wave basis energy cutoff is set to 350 eV. A 100-atom simulation cell is used to model the Σ5(210) GB in $CsPbBr_3$ containing a Pb interstitial, Figure 1. The ab initio training data are collected from MD trajectories obtained using the Γ k-point for computational efficiency. The geometry optimization and electronic structure calculations for structures selected from the ML FF trajectories are performed using a 3×2×1 Γ-centered k-point Monkhorst-Pack mesh to increase the precision, with more k-points corresponding to shorter simulation cell dimensions. After the geometry optimization, we sample ab initio geometries over a wide range of temperatures by performing MD simulations at temperatures ranging from 100 K to 1600 K. Such broad temperature range used to obtain the training data increases diversity of atomic configurations and ensures that distortions and fluctuations of the GB occurring on nanosecond timescales at ambient temperature can be sampled by the shorter ab initio simulations. Lammps[67] is employed to carry MD simulations with the pre-trained ML FF. A 1.5 ns MD trajectory is obtained in the canonical ensemble at 300 K, and the electronic structure and geometry

fluctuation along the trajectory are examined. Single point ab initio calculations are carried out every 10 ps for the whole trajectory. Additionally, two regions, 0.497-0.503 ns and 1.150-1.153 ns, representing different behaviors, Figure 1, are investigated in detail with a 2 fs timestep. The ab initio and ML potential energies are compared to validate the quality of the ML FF, and the root mean squared error is calculated to be 6.58 meV**,** within the recommendation accuracy.[68] As shown in Figure S1, the ML predicted potential energy closely follows the ab initio potential energy.

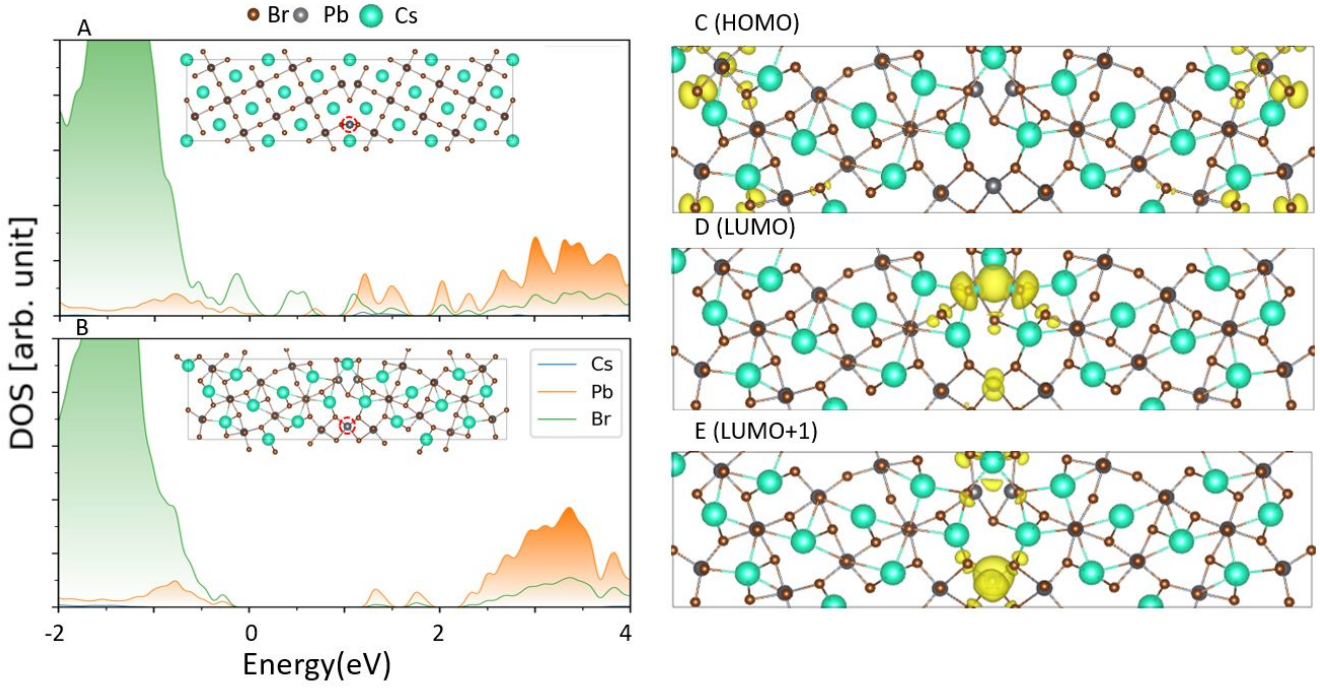

Figure 1. (A) Density of states (DOS) of the unoptimized $CsPbBr_3$ Σ5(210) grain boundary (GB) with Pb interstitial (Pb_i). **(B)** DOS of the optimized system. The corresponding structures are shown in the inserts in (A) and (B). Marked by the red dashed circle, Pb_i is introduced between two Br atoms at the GB. After the optimization, Pb_i is coordinated by Br atoms and makes a stable -Pb-Br-Pb-Br-Pb- structure. **(C)** HOMO, **(D)** LUMO, and **I** LUMO+1 charge densities for the optimized structure. LUMO and LUMO+1 are electron traps, localized, respectively, on the Pb-Pb dimer present in the GB already prior to introduction of Pb_i, and on the introduced Pb_i. Note that there are two GBs in the system, in the middle and at the edges. HOMO is localized on iodines at the other GB and is a very shallow hole trap. Thus, the electron and hole are localized on different GBs and are separated.

3. Results and Discussion

We focus on the $CsPbBr_3$ perovskite that is stable and allows multiple morphologies, including nanocrystals, single crystals, and bulk films. Among these, $CsPbBr_3$ nanocrystals achieve a remarkable maximum photoluminescence quantum yield (PLQY) of 95%. In contrast, other halide perovskites, such as $CsPbI_3$ and $CsPbCl_3$, exhibit lower PLQY values of 70% and 10%, respectively.[69, 70] $CsPbI_3$ has been extensively studied for various applications, however, it faces significant stability challenges.[71] In contrast, $CsPbBr_3$ is more stable at ambient temperatures. The perovskite phase of $CsPbI_3$, which is crucial for its performance, remains stable only at elevated temperatures. Under ambient conditions, $CsPbI_3$ undergoes an unfavorable phase transition to a non-perovskite structure. Combined with moisture exposure, this limits severely the $CsPbI_3$ potential as an efficient material for solar cell devices. The Σ5-(210) and Σ5(210) GBs due are known to have low formation energies,[41, 49] and have been reported experimentally and are widely studied.[37, 38, 72, 73] We focus on the Σ5(210) GB in the $CsPbBr_3$ perovskite and introduce a Pb_i that is known to create deep trap states in bulk regions of MHPs.[48] We place the extra Pb between two Br atoms at the GB, as shown in the insert of Figure 1A, to allow an opportunity for defect healing. Indeed, upon geometry optimization the extra Pb atom creates bonds with more bromines, insert in Figure 1B. The DOS of the unoptimized GB containing Pb_i exhibits many trap states, both deep and shallow. The trap states originate from under-coordinated Pb atoms and lattice mismatch at the GB, inducing multiple dangling bonds. Analysis of the contributions of atomic orbitals to the DOS indicates that the valence band (VB) of $CsPbBr_3$ is formed by antibonding hybridization between the Br 4p and Pb 6s orbitals, while the conduction band (CB) is supported by the Pb 6p and Br 4p orbitals,[74] with the primary contributions to the VB and CB provided by the Br and Pb atomic orbitals, respectively. Cs atoms do not contribute to the electronic states near the band edges, and therefore, they do not participate directly in charge transport, trapping and recombination. Nevertheless, mechanical and electrostatic interactions between Cs atoms and $PbBr_s$ octahedra play important roles and should not be neglected.

Most of the midgap states seen in the unoptimized system disappear after geometry optimization, demonstrating the ability of the GB to heal, Figure 1B. Nevertheless, a shallow hole trap and two deep electron traps remain after the geometry optimization. Parts C-E of Figure 1 show the charge densities of these states, which correspond to the highest occupied molecular orbital (HOMO), lowest unoccupied molecular orbital (LUMO), and LUMO+1. Note that there exists two GBs in the simulation cell, in the middle and at the edges of the structure, due to the periodic boundary conditions. The hole trap and the electron traps are localized on the opposite GBs, indicating that GBs, surfaces, and edges can help separate positive and negative charges, leading to dissociation of photogenerated excitons and helping to prolong

charge carrier lifetimes.[75-78] The symmetry breaking, induced by GBs, also activate new phonon modes that can couple to the electronic degrees of freedom.[38, 76] The shallow hole trap, HOMO, is spread on multiple Br atoms of the outer GB. The electron traps, LUMO and LUMO+1, are localized on Pb atoms in the inner GB. The deeper electron trap, LUMO, is supported by the Pb-Pb dimer observed in the optimized GB even in the absence of the Pb_i defect,[41, 42] suggesting that point defects may play minor roles at GBs, even if they create critical trap states in the bulk.[48] There is an important difference, though. The Pb-Pb distance in the dimer seen in the optimized structure of the stoichiometric Σ5(210) GB is 6.3 Å,[41, 42] while the same Pb-Pb dimer distance in the Σ5(210) GB with Pb_i is much shorter, around 3 Å. Because Pb-Pb distance correlates very strongly with the defect state energy,[79-81] the Pb-Pb dimer state is inside the CB in the stoichiometric Σ5(210) GB, while it is 1 eV below the CB minimum in the Σ5(210) GB with Pb_i. Thus, Pb_i has an important influence on GB structural properties that translate into changes in the electronic structure. Such influence will be seen in the nanosecond evolution of the structural and electronic properties discussed below.

The shallower electron trap is localized on the introduced Pb_i atom, even though it is coordinated by multiple bromines, Figure 1E. The situation is similar to that in bulk $CsPbBr_3$, in which Pb_i also introduces a shallow electron trap near the CB edge, and a state inside the CB.[48] Over time, the GB undergoes significant structural evolution, and the above observations made for the optimized GB structure undergo a significant change, highlighting the need for thorough canonical sampling of MHP structures.

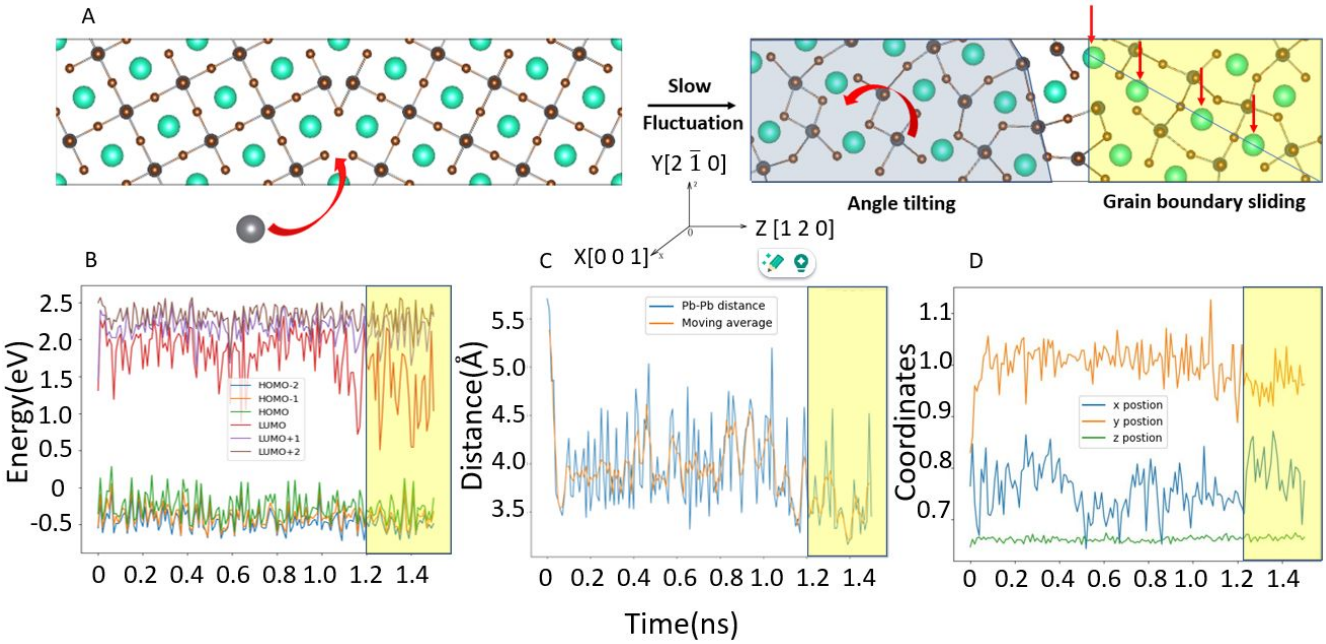

Figure 2. **(A)** Illustration of the simulation process. A Pb_i is introduced between bromine atoms at the GB. Within tens of picoseconds the GB deforms by tilting, Figure 3. After fluctuating for a nanosecond, the GB slides, causing significant changes in the electronic properties, part B. **(B)** Energy level fluctuations along the 1.5 ns trajectory. Ab initio calculations are performed every 10 ps. The LUMO drops every 0.4 ns, at 0.1 ns and 0.5 ns. Then, around 1.1 ns, the GB starts sliding, and the LUMO drops in energy by over 1 eV, creating a deep trap that persists for the rest of the simulation (yellow box). **(C)** Evolution of the distance between the two Pb atoms, marked by blue circles in Figure S3. The distance decreases when the LUMO in part B becomes a deep trap. **(D)** Averaged fractional coordinates of the Cs atoms marked by red circles in Figure S3.

Next, we investigate the long-time dynamics of the Σ5(210) GB with Pb_i at ambient temperature, Figure 2. The 1.5 ns simulation demonstrates three distinct regimes. Within 10 ps, the GB undergoes a structural evolution, identified as tilting in Figure 3. The bonding pattern in the GB region changes significantly, as characterized by the Pb-Pb distance and Cs atom coordinates, Figure 2C,D. During this initial short period, the LUMO energy increases by about 0.5 eV, and the HOMO energy drops, opening up the bandgap. Over the next nanosecond, the GB oscillates around a local equilibrium geometry. The bandgap and Pb-Pb distance remain relatively stable, Figure 3B-C. Starting at 1.1 ns a new deformation is observed, associated with GB sliding, as indicated by the yellow shaded regions in Figure 2. The Pb-Pb distance shortens, and the LUMO energy decreases significantly. Importantly, the deep LUMO level persists for several hundred picoseconds, creating a stable deep trap state. This is in contrast to the

behavior of the same GB without the Pb_i point defect,[41, 42] in which case a GB deformation leads to formation of transient deep traps only. A closer examination of the evolution of LUMO in Figure 2B indicates that a deep trap forms at 0.1 ns and 0.5 ns, but only for a brief time-period. After 1.2 ns, the deep trap persists and becomes particularly deep every 50 ps. The persistence of the deep electron trap level over hundreds of picoseconds can have a strong detrimental effect on charge carrier lifetime and mobility, and hence, material performance.

The data presented in parts A-C of Figure S4 demonstrate that that Cs, Pb, and Br atoms fluctuate collectively. In particular, the data identify point to atomic structure rearrangements occurring at the beginning of the trajectory and at around 1.1 ns. Parts D and E of Figure S4 show evolutions of the distances between the Pb atoms in the Pb trimer. Initially, the distances shorten sharply. Then, they oscillate and shorten again after 1.1 ns, which makes the trimer mid-gap state permanent, Figure 2B. Parts F and G of Figure S4 show the Pb pairs in the sub-boundary region. The Pb pairs tend to form split interstitials and become undersaturated.

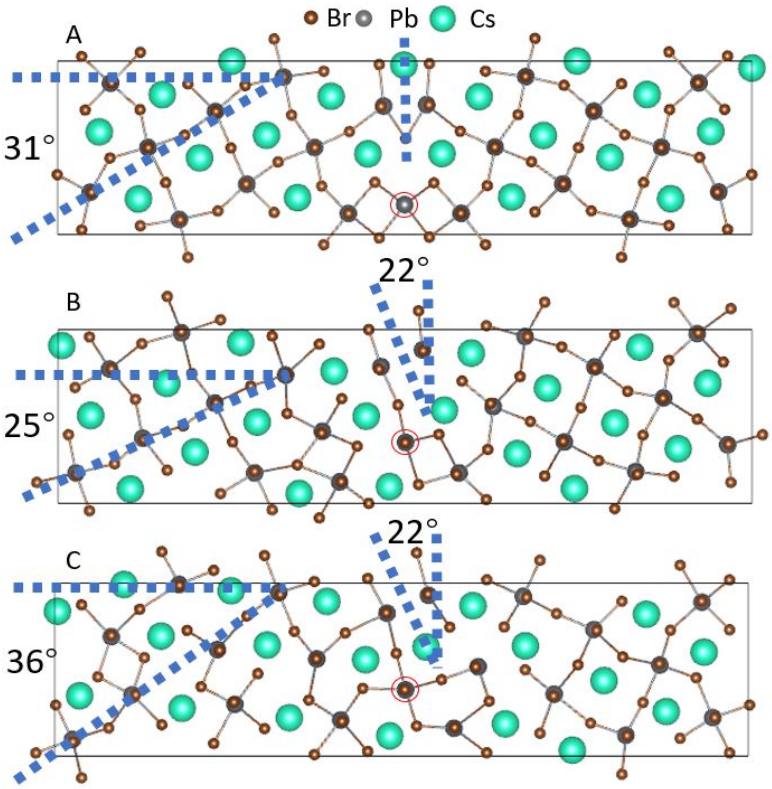

Figure 3. Geometric structures of $CsPbBr_3$ Σ5(210) GB with Pb_i at **(A)** 0 ps, **(B)** 20 ps, and **(C)** 40 ps after the canonical MD simulation is started from the optimized GB. Pb_i is circled with red. The left side of the system tilts

with respect to the middle, as indicated by increase of the middle angle from 0° to 22°. The tilting is accompanied by compression, followed by relaxation: the left side angle changes from 31° to 23° and back to 36°. Subsequently for about 1 ns, the GB fluctuates around the configuration shown in part C, and then starts sliding, Figures 2 and S2. The ~20 ps tilting processes distorts the -Pb-Br-Pb-Br-Pb- structure associated with Pb_i, seen in the optimized structure, part A, however, the Pb-Pb dimer creating the deep trap state, Figure 1D, persists. Eventually a Pb-Pb-Pb trimer is formed, Figure 4, generating persistent midgap trap state that becomes particularly deep when the GB starts sliding after 1.1 ns, Figure 2B.

Figure 3 illustrates geometric changes occurring in the GB within the first 40 ps. In the optimized structure, part A, the system is symmetrical around the y-axis, and the Pb interstitial resides in the middle of the GB. MHPs are soft and can undergo slow large-scale motions around defects,[41, 42, 81-83] and we observe such behavior. By 20 ps, the structure in the middle rotates by 22°. At the same time, the structure on the left side compresses,[84] as indicated by the decrease of the corresponding angle from 31° to 25°. Subsequently, the compression is relaxed, and by 40 ps, the angle on the left is restored back to 36°, while the angle in the middle remains at 22°, Figure 3C.

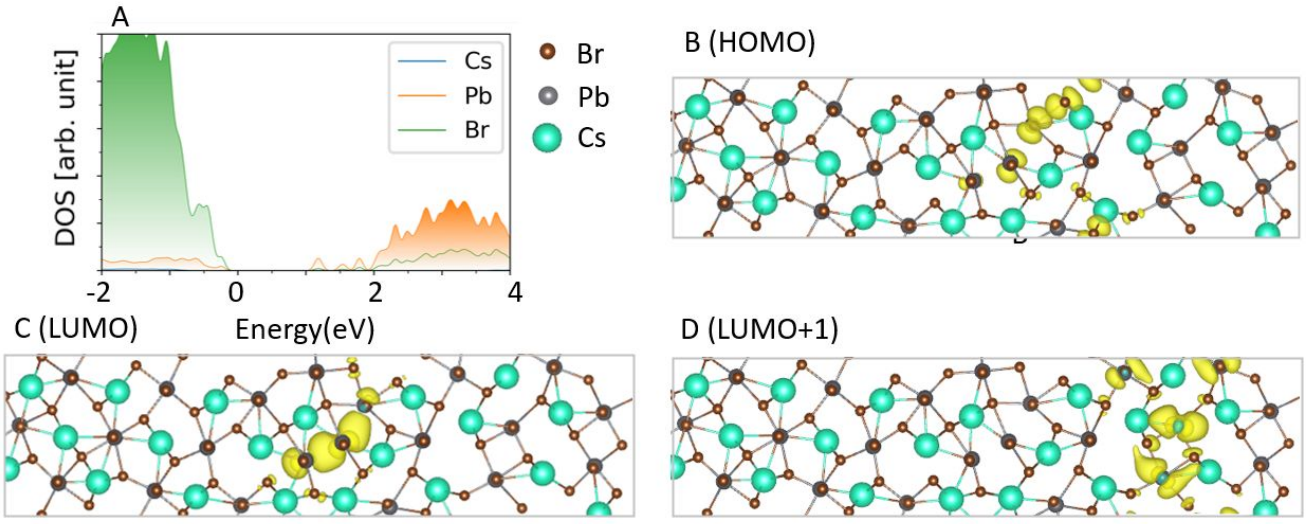

Figure 4. (A) Representative density of states (DOS) at 498,557 fs, selected to show mid-gap trap states. Charge density of **(B)** HOMO, **(C)** LUMO, **(D)** LUMO + 1. The LUMO is a deep trap state formed by a Pb-Pb-Pb trimer forms upon the rapid initial GB reconstruction and remains stable for a long time. The LUMO+1 is a shallow trap

level, formed by a -Pb-Br-Pb-Br-Pb- structure. It is localized in a GB sublayer rather than the GB. Although the HOMO is localized on a few bromines, it should not be regarded as a detrimental trap state, since it is energetically close to the VBM.

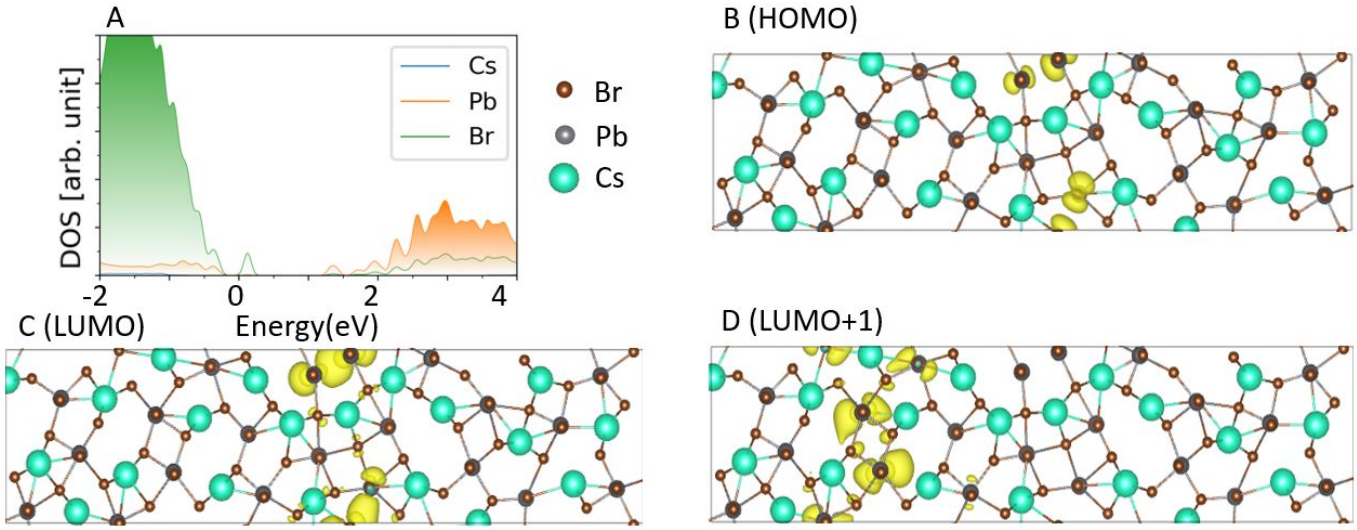

Figure 5. (A) Representative DOS at 1,152,171 fs. Charge densities of **(B)** HOMO, **(C)** LUMO, and **(D)** LUMO + 1. In this example, the HOMO is energetically separated from the VBM and forms a hole trap. Both HOMO and LUMO are localized in the same GB area, forming a bound electron-hole pair. The LUMO+1 is a shallow trap localized in a GB sublayer, similarly to Figure 4D.

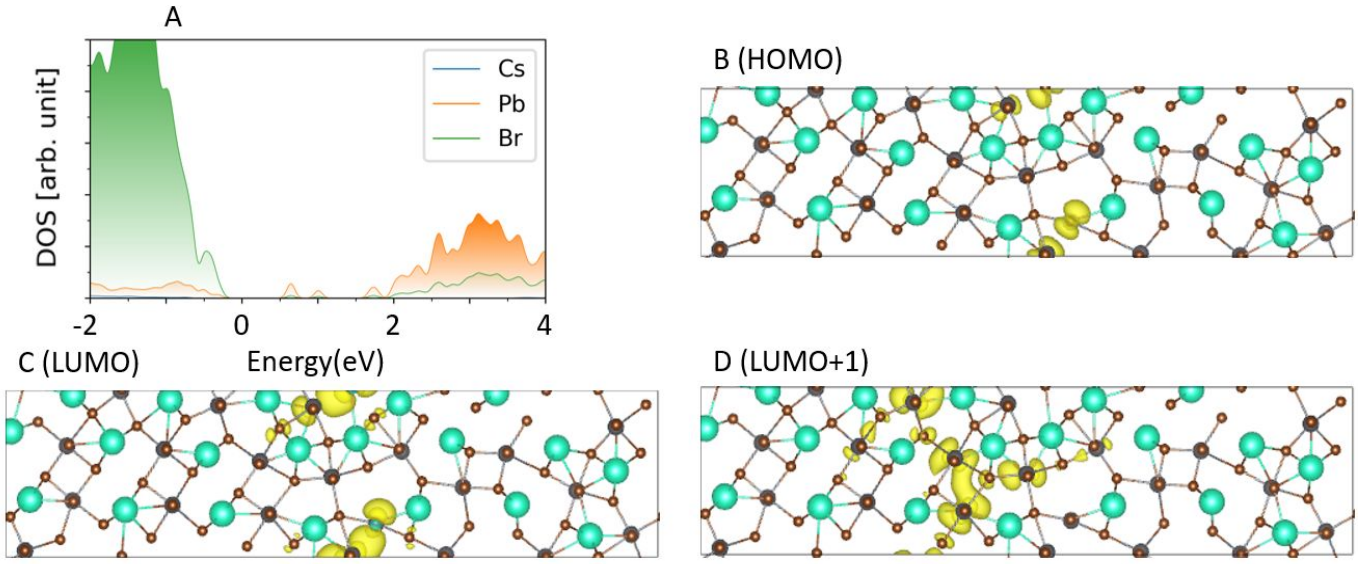

Figure 6. (A) Representative DOS at 1,165,050 fs, showing a very deep electron trap. Charge densities of **(B)** HOMO, **(C)** LUMO, and **(D)** LUMO + 1. Localized on few atoms, the HOMO is very close in energy to the VBM.

The deep trap LUMO is formed by the Pb-Pb-Pb trimer. The LUMO+1 is localized on several Pb atoms connected by Br atoms.

To analyze the origin of the trap states observed in the two regimes of the GB behavior, before and after 1.1 ns, Figure 2, we study the electronic properties with a finer time resolution during the 0.497ns–0.503ns and 1.150ns–1.153ns time-periods. Comparison of the ab initio and ML potential energies can be found in Figure S1B-C. Figures 4 and S3 illustrate the electronic properties in the regime when deep trap states appear only transiently. Recall that the optimized GB structure exhibits two electron traps, Figure 1B. The deeper trap arises from the Pb-Pb dimer that is present in the GB without Pb_i. The shallower trap is formed by the -Pb-Br-Pb-Br-Pb- structure involving Pb_i. The situation is entirely different at ambient temperature, Figure 4. The LUMO is a deep trap state. It is now formed by a Pb-Pb-Pb trimer that involves Pb_i, Figure 4C. Pb-Pb-Pb trimers are known to form stable chemical species.[49] The Pb-Pb distances in the Pb-Pb-Pb trimer are significantly shorter than the Pb-Pb distances in the -Pb-Br-Pb-Br-Pb- structure, and a short Pb-Pb distance gives rise to deep traps.[79-81] The LUMO+1 is a shallower trap. It is localized on several Pb atoms that do not create Pb-Pb dimers but form a distorted structure in a sub-GB layer. The DOS examples of Figure S5 demonstrate that the shallow traps can disappear and that the deep trap can become shallow, however, the Pb-Pb-Pb trimer defect state always remains inside the bandgap. This is in contrast to the properties of the Pb-Pb dimer defect in the GB without Pb_i.[41, 42] Without the Pb_i point defect, the GB can heal, attaining configurations without midgap trap states.

Figures 5, 6 and S6 illustrate electronic properties from the latter part of the trajectory, after the sliding deformation creates persistent deep trap states, Figure 1. Figure 5 presents a geometry in which both electron and hole trap states appear inside the bandgap. The LUMO is an electron trap. It is localized on the Pb-Pb-Pb trimer, which is split vertically due to periodic boundary conditions, Figure 5C. The HOMO is a hole trap. It is localized on Br atoms in the same part of the GB as the HOMOS, Figure 5B. Such configuration favors strong electron-hole interaction and can lead to rapid nonradiative charge recombination. The LUMO+1 is localized on several Pb atoms forming a distorted structure in a sub-GB layer, similarly to Figure 4D. Figure 6 presents a situation with very deep electron traps. Once again, the LUMO is the deeper trap, localized on the Pb-Pb-Pb trimer involving the Pb_i atom. Now the LUMO+1 is also a deep trap, localized on several Pb atoms forming a distorted structure at the GB.

Overall, the appearance of trap states depends on an interplay of the strain, created by structural distortions at the GB, with formation of new, stable chemical species.[79, 80, 85] Pb-Pb dimers can form relatively stable chemical bonds that are not seen in perfect MHP structures but appear in defective structures. At low Pb concentrations, e.g., with stoichiometric compositions in the absence of Pb_i point defects, Pb-Pb bonds form only transiently, and release of the strain by GB healing towards the pristine MHP structure. As the concentration of Pb atoms increases, e.g., with Pb_i point defects, formation of Pb-Pb bonds becomes more likely and cannot be avoided by GB healing towards the pristine structure. Similar phenomena can occur with other point defects, such as halide interstitials and atom replacements, e.g., replacement of Cs with Pb. Whether or not the newly form species create midgap charge trap states depends on the electronic properties of the species. Creation of new chemical structures becomes much more likely at GBs, in which the pristine structure is already distorted due to strain. The trap states created by Pb dimers and trimers generate midgap trap states that can be eliminated by excess halide atoms, which break Pb-Pb bonds, and other chemical passivation strategies.[46, 86-95]

3. Conclusions

We have demonstrated that point defects at MHP GBs can create new chemical species, e.g., Pb-Pb-Pb trimers, that are less likely to occur with point defects in bulk. Depending on the electronic properties of the species, midgap trap states can appear, and influence charge carrier mobility and lifetime. We have also demonstrated that MHP GBs can undergo slow structural fluctuations on nanosecond timescales, comparable to charge carrier lifetimes. Often, structural fluctuations enhance oscillations of defect state energies, such that deep defect levels can become shallow, e.g., due to transient breaking of Pb-Pb bonds, and trapped charges can escape into bands and participate again in charge transport. On the other hand, point defects can create stable local structures at GBs, and result in persistent deep midgap traps that can strongly decrease carrier lifetime and mobility. Overall, the appearance of trap states depends on interplay between the healing of structural distortions at the GB towards the pristine structure and formation of new stable chemical species that prevent the healing. Furthermore, such chemical species can lead to structural instabilities at GBs and slow structural evolution.

The reported analysis has been made possible by development of a ML FF, which allowed us to sample nanosecond structural dynamics, with subsequent ab initio analysis of electronic structure of representative GB conformations. Development of a FF for description of MHP GBs is challenging,

because the region is nearly amorphous, and a traditional FF or a ReaxFF may not capture all chemical structures possible in GBs. Development of a ML FF for MHP GBs is also a challenging task, because configurations encountered at GBs may differ very significant from equilibrium configurations in pristine MHPs.

The structural evolution of the studied $CsPbBr_3$ Σ5(210) GB with the Pb interstitial defect exhibits a fast, 10 ps component and a slow nanosecond dynamics. The fast component is associated with healing of the local GB structure and involves GB tilting, sliding and rearrangement of chemical bonds in the GB region. The nanosecond evolution involves GB sliding and results in formation of deep trap states that persists for hundreds of picoseconds and strongly decrease charge carrier mobility and lifetime. Initially, deeper traps are associated with Pb-Pb dimers that are present in the GB even without the Pb interstitial, while shallower traps are associated with -Pb-Br-Pb-Br-Pb- type structures. After the fast GB restructuring, a Pb-Pb-Pb trimer forms creating a deep trap. In contrast to the Pb-Pb dimer that can be broken by GB fluctuations, the Pb-Pb-Pb trimer cannot be fully dissociated, and as result, the deep trap persists continuously. Furthermore, the GB sliding observed after a 1 ns evolution make the Pb-Pb-Pb trimer trap particularly deep for at least 300 ps. Other, shallow trap states associated with distorted structures are seen in sub-boundary layers, which are jammed in unfavorable conformations. The persistent deep trap state of the Pb-Pb-Pb trimer can only be broken by chemical means, such as introduction of excess halide that can break Pb-Pb bonds, emphasizing the importance of developing efficient defect passivation strategies. The nanosecond analysis of the geometric and electronic structure of MHP defects highlights that complex, multiscale nature of MHP dynamics, and complex interplay between ion and charge dynamics.

Acknowledgements.

O.V.P. acknowledges the support of the US Department of Energy, grant DE-SC0014429.

Supporting Information.

Comparison of ab initio and machine learning potential energies, and representative atomic configurations and densities of states. CIF structure files. The Supporting Information is available free of charge.

References.

(1) Turren-Cruz, S.-H.; Saliba, M.; Mayer, M. T.; Juárez-Santiesteban, H.; Mathew, X.; Nienhaus, L.; Tress, W.; Erodici, M. P.; Sher, M.-J.; Bawendi, M. G., Enhanced Charge Carrier Mobility and Lifetime Suppress Hysteresis and Improve Efficiency in Planar Perovskite Solar Cells. *Energy & Environmental Science* **2018**, *11*, 78-86.
(2) Oga, H.; Saeki, A.; Ogomi, Y.; Hayase, S.; Seki, S., Improved Understanding of the Electronic and Energetic Landscapes of Perovskite Solar Cells: High Local Charge Carrier Mobility, Reduced Recombination, and Extremely Shallow Traps. *Journal of the American Chemical Society* **2014**, *136*, 13818-13825.
(3) Kaur, G.; Shukla, A.; Sinha, A.; Debnath, K.; Babu, K. J.; Bhatt, H.; Waghmare, U. V.; Ghosh, H. N., Ultrafast Glimpses of the Excitation Energy-Dependent Exciton Dynamics and Charge Carrier Mobility in Cs₂Sni₆ Nanocrystals. *Nanoscale* **2023**, *15*, 14081-14092.
(4) Ning, W.; Wang, F.; Wu, B.; Lu, J.; Yan, Z.; Liu, X.; Tao, Y.; Liu, J. M.; Huang, W.; Fahlman, M., Long Electron–Hole Diffusion Length in High-Quality Lead-Free Double Perovskite Films. *Advanced Materials* **2018**, *30*, 1706246.
(5) Stranks, S. D.; Eperon, G. E.; Grancini, G.; Menelaou, C.; Alcocer, M. J.; Leijtens, T.; Herz, L. M.; Petrozza, A.; Snaith, H. J., Electron-Hole Diffusion Lengths Exceeding 1 Micrometer in an Organometal Trihalide Perovskite Absorber. *Science* **2013**, *342*, 341-344.
(6) Shi, D.; Adinolfi, V.; Comin, R.; Yuan, M.; Alarousu, E.; Buin, A.; Chen, Y.; Hoogland, S.; Rothenberger, A.; Katsiev, K., Low Trap-State Density and Long Carrier Diffusion in Organolead Trihalide Perovskite Single Crystals. *Science* **2015**, *347*, 519-522.
(7) Jiang, N.; Ma, G. Q.; Song, D. D.; Qiao, B.; Liang, Z. Q.; Xu, Z.; Wageh, S.; Al-Ghamdi, A.; Zhao, S. L., Defects in Lead Halide Perovskite Light-Emitting Diodes under Electric Field: From Behavior to Passivation Strategies. *Nanoscale* **2024**, *16*, 3838-3880.
(8) Yin, W.-J.; Shi, T.; Yan, Y., Unusual Defect Physics in Ch3nh3pbi3 Perovskite Solar Cell Absorber. *Applied Physics Letters* **2014**, *104*, 063903.
(9) Li, W.; She, Y. L.; Vasenko, A. S.; Prezhdo, O. V., <I>Ab Initio</I> Nonadiabatic Molecular Dynamics of Charge Carriers in Metal Halide Perovskites. *Nanoscale* **2021**, *13*, 10239-10265.
(10) Meng, X.; Jia, Z. R.; Niu, X. X.; He, C. N.; Hou, Y., Opportunities and Challenges in Perovskite-Organic Thin-Film Tandem Solar Cells. *Nanoscale* **2024**, *16*, 8307-8316.
(11) Dou, L.; Yang, Y.; You, J.; Hong, Z.; Chang, W.-H.; Li, G.; Yang, Y., Solution-Processed Hybrid Perovskite Photodetectors with High Detectivity. *Nature Communications* **2014**, *5*, 5404.
(12) Dupe, S.; Liu, D. Y.; Ghosh, A.; Vasenko, A. S.; Pouget, S.; Schlutig, S.; Vidal, M.; Lebeau, B.; Ling, W. L.; Reiss, P.; Prezhdo, O. V.; Ryzhikov, A.; Aldakov, D., Quantum-Confined Bismuth Iodide Perovskite Nanocrystals in Mesoporous Matrices. *Nanoscale* **2024**, *16*, 11223-11231.
(13) Kundar, M.; Gayen, K.; Ray, R.; Kushavah, D.; Pal, S. K., Highly Stable Two-Dimensional Ruddlesden-Popper Perovskite-Based Resistive Switching Memory Devices. *Nanoscale* **2024**.
(14) Lin, K.; Xing, J.; Quan, L. N.; de Arquer, F. P. G.; Gong, X.; Lu, J.; Xie, L.; Zhao, W.; Zhang, D.; Yan, C.; Li, W.; Liu, X.; Lu, Y.; Kirman, J.; Sargent, E. H.; Xiong, Q.; Wei, Z., Perovskite Light-Emitting Diodes with External Quantum Efficiency Exceeding 20 Per Cent. *Nature* **2018**, *562*, 245-248.
(15) Bi, D.; Xu, B.; Gao, P.; Sun, L.; Grätzel, M.; Hagfeldt, A., Facile Synthesized Organic Hole Transporting Material for Perovskite Solar Cell with Efficiency of 19.8%. *Nano Energy* **2016**, *23*, 138-144.
(16) Wu, Y. L.; Lu, S. H.; Ju, M. G.; Zhou, Q. H.; Wang, J. L., Accelerated Design of Promising Mixed Lead-Free Double Halide Organic-Inorganic Perovskites for Photovoltaics Using Machine Learning. *Nanoscale* **2021**, *13*, 12250-12259.
(17) Paul, T.; Sahoo, A.; Maiti, S.; Mandal, S.; Bhattacharjee, S.; Maity, A.; Chattopadhyay, K. K., Observation of Piezoelectricity in a Lead-Free Cs₂Agbibr₆ Perovskite: A New Entrant in the Energy Harvesting Arena. *Nanoscale* **2024**.

(18) Diez-Cabanes, V.; Even, J.; Beljonne, D.; Quarti, C., Electronic Structure and Optical Properties of Mixed Iodine/Bromine Lead Perovskites. To Mix or Not to Mix? *Advanced Optical Materials* **2021**, *9*, 2001832.
(19) Zheng, J. Y.; Ma, J. W.; Yu, M. H.; Xie, H.; Yan, D. D.; Dong, Y. H.; Liu, Y.; Wang, X. Y.; Ye, W. X., Efficient Open-Air Synthesis of Mg²⁺-Doped Cspbi₃ Nanocrystals for High-Performance Red Leds. *Nanoscale* **2024**, *16*, 14108-14115.
(20) Yang, W. S.; Park, B.-W.; Jung, E. H.; Jeon, N. J.; Kim, Y. C.; Lee, D. U.; Shin, S. S.; Seo, J.; Kim, E. K.; Noh, J. H., Iodide Management in Formamidinium-Lead-Halide–Based Perovskite Layers for Efficient Solar Cells. *Science* **2017**, *356*, 1376-1379.
(21) Smith, J. S.; Isayev, O.; Roitberg, A. E., Ani-1: An Extensible Neural Network Potential with Dft Accuracy at Force Field Computational Cost. *Chem Sci* **2017**, *8*, 3192-3203.
(22) Quarti, C.; De Angelis, F.; Beljonne, D., Influence of Surface Termination on the Energy Level Alignment at the Ch3nh3pbi3 Perovskite/C60 Interface. *Chemistry of Materials* **2017**, *29*, 958-968.
(23) Qiu, X.; Cao, B.; Yuan, S.; Chen, X.; Qiu, Z.; Jiang, Y.; Ye, Q.; Wang, H.; Zeng, H.; Liu, J.; Kanatzidis, M. G., From Unstable Cssni3 to Air-Stable Cs2sni6: A Lead-Free Perovskite Solar Cell Light Absorber with Bandgap of 1.48 Ev and High Absorption Coefficient. *Solar Energy Materials and Solar Cells* **2017**, *159*, 227-234.
(24) Thouin, F.; Valverde-Chávez, D. A.; Quarti, C.; Cortecchia, D.; Bargigia, I.; Beljonne, D.; Petrozza, A.; Silva, C.; Srimath Kandada, A. R., Phonon Coherences Reveal the Polaronic Character of Excitons in Two-Dimensional Lead Halide Perovskites. *Nature materials* **2019**, *18*, 349-356.
(25) Gao, Y.; Wu, Y.; Lu, H.; Chen, C.; Liu, Y.; Bai, X.; Yang, L.; William, W. Y.; Dai, Q.; Zhang, Y., Cspbbr3 Perovskite Nanoparticles as Additive for Environmentally Stable Perovskite Solar Cells with 20.46% Efficiency. *Nano Energy* **2019**, *59*, 517-526.
(26) Wu, Y.; Chu, W.; Vasenko, A. S.; Prezhdo, O. V., Common Defects Accelerate Charge Carrier Recombination in Cssni3 without Creating Mid-Gap States. *The Journal of Physical Chemistry Letters* **2021**, *12*, 8699-8705.
(27) Chung, I.; Song, J.-H.; Im, J.; Androulakis, J.; Malliakas, C. D.; Li, H.; Freeman, A. J.; Kenney, J. T.; Kanatzidis, M. G., Cssni3: Semiconductor or Metal? High Electrical Conductivity and Strong near-Infrared Photoluminescence from a Single Material. High Hole Mobility and Phase-Transitions. *Journal of the american chemical society* **2012**, *134*, 8579-8587.
(28) Mortazavi, B.; Pötschke, M.; Cuniberti, G., Multiscale Modeling of Thermal Conductivity of Polycrystalline Graphene Sheets. *Nanoscale* **2014**, *6*, 3344-3352.
(29) Nie, W.; Tsai, H.; Asadpour, R.; Blancon, J.-C.; Neukirch, A. J.; Gupta, G.; Crochet, J. J.; Chhowalla, M.; Tretiak, S.; Alam, M. A.; Wang, H.-L.; Mohite, A. D., High-Efficiency Solution-Processed Perovskite Solar Cells with Millimeter-Scale Grains. *Science* **2015**, *347*, 522-525.
(30) Wang, F.; Bai, S.; Tress, W.; Hagfeldt, A.; Gao, F., Defects Engineering for High-Performance Perovskite Solar Cells. *npj Flexible Electronics* **2018**, *2*, 1-14.
(31) Shao, Y.; Fang, Y.; Li, T.; Wang, Q.; Dong, Q.; Deng, Y.; Yuan, Y.; Wei, H.; Wang, M.; Gruverman, A.; Shield, J.; Huang, J., Grain Boundary Dominated Ion Migration in Polycrystalline Organic–Inorganic Halide Perovskite Films. *Energy & Environmental Science* **2016**, *9*, 1752-1759.
(32) Park, J.-S.; Calbo, J.; Jung, Y.-K.; Whalley, L. D.; Walsh, A., Accumulation of Deep Traps at Grain Boundaries in Halide Perovskites. *ACS Energy Letters* **2019**, *4*, 1321-1327.
(33) Park, J.-S.; Walsh, A., Modeling Grain Boundaries in Polycrystalline Halide Perovskite Solar Cells. *Annual Review of Condensed Matter Physics* **2021**, *12*, 95-109.
(34) Kaiser, W.; Hussain, K.; Singh, A.; Alothman, A. A.; Meggiolaro, D.; Gagliardi, A.; Mosconi, E.; De Angelis, F., Defect Formation and Healing at Grain Boundaries in Lead-Halide Perovskites. *Journal of Materials Chemistry A* **2022**, *10*, 24854-24865.
(35) Meggiolaro, D.; Mosconi, E.; De Angelis, F., Formation of Surface Defects Dominates Ion Migration in Lead-Halide Perovskites. *ACS Energy Letters* **2019**, *4*, 779-785.

(36) Quilettes, D. W. d.; Vorpahl, S. M.; Stranks, S. D.; Nagaoka, H.; Eperon, G. E.; Ziffer, M. E.; Snaith, H. J.; Ginger, D. S., Impact of Microstructure on Local Carrier Lifetime in Perovskite Solar Cells. *Science* **2015**, *348*, 683-686.
(37) Wang, Y.; He, J.; Yang, Y.; Zhang, Z.; Long, R., Chlorine Passivation of Grain Boundary Suppresses Electron–Hole Recombination in Cspbbr3 Perovskite by Nonadiabatic Molecular Dynamics Simulation. *ACS Applied Energy Materials* **2019**, *2*, 3419-3426.
(38) Long, R.; Liu, J.; Prezhdo, O. V., Unravelling the Effects of Grain Boundary and Chemical Doping on Electron–Hole Recombination in Ch3nh3pbi3 Perovskite by Time-Domain Atomistic Simulation. *Journal of the American Chemical Society* **2016**, *138*, 3884-3890.
(39) Im, J.-H.; Jang, I.-H.; Pellet, N.; Grätzel, M.; Park, N.-G., Growth of Ch3nh3pbi3 Cuboids with Controlled Size for High-Efficiency Perovskite Solar Cells. *Nature Nanotechnology* **2014**, *9*, 927-932.
(40) Ren, X.; Yang, Z.; Yang, D.; Zhang, X.; Cui, D.; Liu, Y.; Wei, Q.; Fan, H.; Liu, S., Modulating Crystal Grain Size and Optoelectronic Properties of Perovskite Films for Solar Cells by Reaction Temperature. *Nanoscale* **2016**, *8*, 3816-3822.
(41) Guo, Y.; Wang, Q.; Saidi, W. A., Structural Stabilities and Electronic Properties of High-Angle Grain Boundaries in Perovskite Cesium Lead Halides. *The Journal of Physical Chemistry C* **2017**, *121*, 1715-1722.
(42) Yang, M.; Zeng, Y.; Li, Z.; Kim, D. H.; Jiang, C.-S.; Van De Lagemaat, J.; Zhu, K., Do Grain Boundaries Dominate Non-Radiative Recombination in Ch 3 Nh 3 Pbi 3 Perovskite Thin Films? *Physical Chemistry Chemical Physics* **2017**, *19*, 5043-5050.
(43) Liu, D. Y.; Wu, Y. F.; Vasenko, A. S.; Prezhdo, O. V., Grain Boundary Sliding and Distortion on a Nanosecond Timescale Induce Trap States in Cspbbr3: Ab Initio Investigation with Machine Learning Force Field. *Nanoscale* **2022**, *15*, 285-293.
(44) Wu, Y. F.; Liu, D. Y.; Chu, W. B.; Wang, B. P.; Vasenko, A. S.; Prezhdo, O. V., Fluctuations at Metal Halide Perovskite Grain Boundaries Create Transient Trap States: Machine Learning Assisted Ab Initio Analysis. *Acs Applied Materials & Interfaces* **2022**, *14*, 55753–55761.
(45) Liu, D. Y.; Wu, Y. F.; Samatov, M. R.; Vasenko, A. S.; Chulkov, E. V.; Prezhdo, O. V., Compression Eliminates Charge Traps by Stabilizing Perovskite Grain Boundary Structures: An Ab Initio Analysis with Machine Learning Force Field. *Chemistry of Materials* **2024**, *36*, 2898-2906.
(46) Qiao, L.; Fang, W. H.; Long, R.; Prezhdo, O. V., Atomic Model for Alkali Metal Passivation of Point Defects at Perovskite Grain Boundaries. *Acs Energy Letters* **2020**, *5*, 3813-3820.
(47) Ran, J. Y.; Wang, B. P.; Wu, Y. F.; Liu, D. Y.; Perez, C. M.; Vasenko, A. S.; Prezhdo, O. V., Halide Vacancies Create No Charge Traps on Lead Halide Perovskite Surfaces but Can Generate Deep Traps in the Bulk. *Journal of Physical Chemistry Letters* **2023**, *14*, 6028-6036.
(48) Kang, J.; Wang, L.-W., High Defect Tolerance in Lead Halide Perovskite Cspbbr3. *The Journal of Physical Chemistry Letters* **2017**, *8*, 489-493.
(49) Shan, W.; Saidi, W. A., Segregation of Native Defects to the Grain Boundaries in Methylammonium Lead Iodide Perovskite. *The Journal of Physical Chemistry Letters* **2017**, *8*, 5935-5942.
(50) Yin, W.-J.; Shi, T.; Yan, Y., Unique Properties of Halide Perovskites as Possible Origins of the Superior Solar Cell Performance. *Advanced Materials* **2014**, *26*, 4653-4658.
(51) Long, R.; Fang, Q.; Vasenko, A. S.; Shi, R.; Fang, W. H.; Prezhdo, O. V., Structural Disorder in Higher-Temperature Phases Increases Charge Carrier Lifetimes in Metal Halide Perovskites. *Journal of the American Chemical Society* **2022**, *144*, 19137-19149.
(52) Yin, J. W.; Xu, Z. F.; Hu, Q.; Teobaldi, G.; Liu, L. M.; Prezhdo, O. V., Tuning Octahedral Tilting by Doping to Prevent Detrimental Phase Transition and Extend Carrier Lifetime in Organometallic Perovskites. *Journal of the American Chemical Society* **2023**, *145*, 5393–5399.
(53) Nan, G.; Zhang, X.; Abdi-Jalebi, M.; Andaji-Garmaroudi, Z.; Stranks, S. D.; Lu, G.; Beljonne, D., How Methylammonium Cations and Chlorine Dopants Heal Defects in Lead Iodide Perovskites. *Advanced Energy Materials* **2018**, *8*, 1702754.

(54) Yun, J. S.; Seidel, J.; Kim, J.; Soufiani, A. M.; Huang, S.; Lau, J.; Jeon, N. J.; Seok, S. I.; Green, M. A.; Ho-Baillie, A., Critical Role of Grain Boundaries for Ion Migration in Formamidinium and Methylammonium Lead Halide Perovskite Solar Cells. *Advanced Energy Materials* **2016**, *6*, 1600330.
(55) Liu, Z.; Wu, C. T.; Koishi, M., Transfer Learning of Deep Material Network for Seamless Structure–Property Predictions. *Computational Mechanics* **2019**, *64*, 451-465.
(56) Feng, S.; Zhou, H.; Dong, H., Application of Deep Transfer Learning to Predicting Crystal Structures of Inorganic Substances. *Computational Materials Science* **2021**, *195*, 110476.
(57) Oda, H.; Kiyohara, S.; Tsuda, K.; Mizoguchi, T., Transfer Learning to Accelerate Interface Structure Searches. *Journal of the Physical Society of Japan* **2017**, *86*, 123601.
(58) Liu, D. Y.; Wang, B. P.; Wu, Y. F.; Vasenko, A. S.; Prezhdo, O., Breaking the Size Limitation of Nonadiabatic Molecular Dynamics in Condensed Matter Systems with Local Descriptor Machine Learning. *Proceedings of the National Academy of Sciences of the United States of America* **2024**, *121*.
(59) Wang, H.; Zhang, L.; Han, J.; E, W., Deepmd-Kit: A Deep Learning Package for Many-Body Potential Energy Representation and Molecular Dynamics. *Computer Physics Communications* **2018**, *228*, 178-184.
(60) Smith, J. S.; Nebgen, B. T.; Zubatyuk, R.; Lubbers, N.; Devereux, C.; Barros, K.; Tretiak, S.; Isayev, O.; Roitberg, A. E., Approaching Coupled Cluster Accuracy with a General-Purpose Neural Network Potential through Transfer Learning. *Nature Communications* **2019**, *10*, 2903.
(61) Kresse, G.; Furthmüller, J., Efficient Iterative Schemes for Ab Initio Total-Energy Calculations Using a Plane-Wave Basis Set. *Physical Review B* **1996**, *54*, 11169-11186.
(62) Perdew, J. P.; Burke, K.; Ernzerhof, M., Generalized Gradient Approximation Made Simple. *Physical review letters* **1996**, *77*, 3865.
(63) Blöchl, P. E., Projector Augmented-Wave Method. *Physical Review B* **1994**, *50*, 17953-17979.
(64) Meggiolaro, D.; De Angelis, F., First-Principles Modeling of Defects in Lead Halide Perovskites: Best Practices and Open Issues. *Acs Energy Letters* **2018**, *3*, 2206-2222.
(65) Deng, L. J.; Ran, J. Y.; Wang, B. P.; Boziki, A.; Tkatchenko, A.; Jiang, J.; Prezhdo, O. V., Strong Dependence of Point Defect Properties in Metal Halide Perovskites on Description of Van Der Waals Interaction. *Journal of Physical Chemistry Letters* **2024**, *15*, 10465-10472.
(66) Grimme, S.; Antony, J.; Ehrlich, S.; Krieg, H., A Consistent and Accurate Ab Initio Parametrization of Density Functional Dispersion Correction (Dft-D) for the 94 Elements H-Pu. *The Journal of chemical physics* **2010**, *132*, 154104.
(67) Thompson, A. P.; Aktulga, H. M.; Berger, R.; Bolintineanu, D. S.; Brown, W. M.; Crozier, P. S.; in 't Veld, P. J.; Kohlmeyer, A.; Moore, S. G.; Nguyen, T. D.; Shan, R.; Stevens, M. J.; Tranchida, J.; Trott, C.; Plimpton, S. J., Lammps - a Flexible Simulation Tool for Particle-Based Materials Modeling at the Atomic, Meso, and Continuum Scales. *Computer Physics Communications* **2022**, *271*, 108171.
(68) Wen, T.; Zhang, L.; Wang, H.; E, W.; Srolovitz, D. J., Deep Potentials for Materials Science. *Materials Futures* **2022**, *1*, 022601.
(69) Wang, K.; Jin, Z.; Liang, L.; Bian, H.; Bai, D.; Wang, H.; Zhang, J.; Wang, Q.; Liu, S., All-Inorganic Cesium Lead Iodide Perovskite Solar Cells with Stabilized Efficiency Beyond 15%. *Nature Communications* **2018**, *9*, 4544.
(70) Ullah, S.; Wang, J.; Yang, P.; Liu, L.; Yang, S.-E.; Xia, T.; Guo, H.; Chen, Y., All-Inorganic Cspbbr 3 Perovskite: A Promising Choice for Photovoltaics. *Materials Advances* **2021**, *2*, 646-683.
(71) Zhao, X.; Vasenko, A. S.; Prezhdo, O.; Long, R., Anion Doping Delays Nonradiative Electron-Hole Recombination in Cs-Based All-Inorganic Perovskites: Time Domain Ab Initio Analysis. *Journal of Physical Chemistry Letters* **2022**, *13*, 11375-11382.
(72) Thind, A. S.; Luo, G.; Hachtel, J. A.; Morrell, M. V.; Cho, S. B.; Borisevich, A. Y.; Idrobo, J.-C.; Xing, Y.; Mishra, R., Atomic Structure and Electrical Activity of Grain Boundaries and Ruddlesden–Popper Faults in Cesium Lead Bromide Perovskite. *Advanced Materials* **2019**, *31*, 1805047.

(73) Pols, M.; Hilpert, T.; Filot, I. A. W.; van Duin, A. C. T.; Calero, S.; Tao, S., What Happens at Surfaces and Grain Boundaries of Halide Perovskites: Insights from Reactive Molecular Dynamics Simulations of Cspbi3. *ACS Applied Materials & Interfaces* **2022**, *14*, 40841-40850.
(74) Xiao, G.; Cao, Y.; Qi, G.; Wang, L.; Liu, C.; Ma, Z.; Yang, X.; Sui, Y.; Zheng, W.; Zou, B., Pressure Effects on Structure and Optical Properties in Cesium Lead Bromide Perovskite Nanocrystals. *Journal of the American Chemical Society* **2017**, *139*, 10087-10094.
(75) Zhang, Z. S.; Fang, W. H.; Long, R.; Prezhdo, O. V., Exciton Dissociation and Suppressed Charge Recombination at 2d Perovskite Edges: Key Roles of Unsaturated Halide Bonds and Thermal Disorder. *Journal of the American Chemical Society* **2019**, *141*, 15557-15566.
(76) Wang, Y. T.; Fang, W. H.; Long, R.; Prezhdo, O. V., Symmetry Breaking at Mapbi(3) Perovskite Grain Boundaries Suppresses Charge Recombination: Time-Domain Ab Initio Analysis. *Journal of Physical Chemistry Letters* **2019**, *10*, 1617-1623.
(77) Shi, R.; Long, R.; Fang, W. H.; Prezhdo, O. V., Rapid Interlayer Charge Separation and Extended Carrier Lifetimes Due to Spontaneous Symmetry Breaking in Organic and Mixed Organic-Inorganic Dion-Jacobson Perovskites. *Journal of the American Chemical Society* **2023**, *145*, 5297–5309.
(78) Shi, R.; Vasenko, A. S.; Long, R.; Prezhdo, O. V., Edge Influence on Charge Carrier Localization and Lifetime in Ch3nh3pbbr3 Perovskite: Ab Initio Quantum Dynamics Simulation. *Journal of Physical Chemistry Letters* **2020**, *11*, 9100-9109.
(79) Agiorgousis, M. L.; Sun, Y.-Y.; Zeng, H.; Zhang, S., Strong Covalency-Induced Recombination Centers in Perovskite Solar Cell Material Ch3nh3pbi3. *Journal of the American Chemical Society* **2014**, *136*, 14570-14575.
(80) Li, W.; Sun, Y. Y.; Li, L. Q.; Zhou, Z. H.; Tang, J. F.; Prezhdo, O. V., Control of Charge Recombination in Perovskites by Oxidation State of Halide Vacancy. *Journal of the American Chemical Society* **2018**, *140*, 15753-15763.
(81) Wang, B. P.; Chu, W. B.; Wu, Y. F.; Casanova, D.; Saidi, W. A.; Prezhdo, O. V., Electron-Volt Fluctuation of Defect Levels in Metal Halide Perovskites on a 100 Ps Time Scale. *Journal of Physical Chemistry Letters* **2022**, *13*, 5946-5952.
(82) Li, W.; Tang, J. F.; Casanova, D.; Prezhdo, O. V., Time-Domain Ab Lnitio Analysis Rationalizes the Unusual Temperature Dependence of Charge Carrier Relaxation in Lead Halide Perovskite. *Acs Energy Letters* **2018**, *3*, 2713-2720.
(83) He, J. L.; Fang, W. H.; Long, R.; Prezhdo, O. V., Increased Lattice Stiffness Suppresses Nonradiative Charge Recombination in Mapbl₃ Doped with Larger Cations: Time Domain Ab Initio Analysis. *Acs Energy Letters* **2018**, *3*, 2070-+.
(84) Ma, X. B.; Fang, W. H.; Long, R.; Prezhdo, O. V., Compression of Organic Molecules Coupled with Hydrogen Bonding Extends the Charge Carrier Lifetime in Ba₂Sni₄. *Journal of the American Chemical Society* **2024**, *146*, 16314-16323.
(85) Liu, D. Y.; Perez, C. M.; Vasenko, A. S.; Prezhdo, O. V., Ag-Bi Charge Redistribution Creates Deep Traps in Defective Cs2agbibr6: Machine Learning Analysis of Density Functional Theory. *Journal of Physical Chemistry Letters* **2022**, *13*, 3645-3651.
(86) Noel, N. K.; Abate, A.; Stranks, S. D.; Parrott, E. S.; Burlakov, V. M.; Goriely, A.; Snaith, H. J., Enhanced Photoluminescence and Solar Cell Performance Via Lewis Base Passivation of Organic Inorganic Lead Halide Perovskites. *Acs Nano* **2014**, *8*, 9815-9821.
(87) Liu, L. H.; Fang, W. H.; Long, R.; Prezhdo, O. V., Lewis Base Passivation of Hybrid Halide Perovskites Slows Electron-Hole Recombination: Time-Domain Ab Lnitio Analysis. *Journal of Physical Chemistry Letters* **2018**, *9*, 1164-1171.
(88) Zheng, X. P.; Chen, B.; Dai, J.; Fang, Y. J.; Bai, Y.; Lin, Y. Z.; Wei, H. T.; Zeng, X. C.; Huang, J. S., Defect Passivation in Hybrid Perovskite Solar Cells Using Quaternary Ammonium Halide Anions and Cations. *Nature Energy* **2017**, *2*, 17102.

(89) Li, W.; Zhan, J.; Liu, X. R.; Tang, J. F.; Yin, W. J.; Prezhdo, O. V., Atomistic Mechanism of Passivation of Halide Vacancies in Lead Halide Perovskites by Alkali Ions. *Chemistry of Materials* **2021**, *33*, 1285-1292.
(90) Abdi-Jalebi, M.; Andaji-Garmaroudi, Z.; Cacovich, S.; Stavrakas, C.; Philippe, B.; Richter, J. M.; Alsari, M.; Booker, E. P.; Hutter, E. M.; Pearson, A. J.; Lilliu, S.; Savenije, T. J.; Rensmo, H.; Divitini, G.; Ducati, C.; Friend, R. H.; Stranks, S. D., Maximizing and Stabilizing Luminescence from Halide Perovskites with Potassium Passivation. *Nature* **2018**, *555*, 497-+.
(91) Qiao, L.; Fang, W. H.; Long, R.; Prezhdo, O. V., Extending Carrier Lifetimes in Lead Halide Perovskites with Alkali Metals by Passivating and Eliminating Halide Interstitial Defects. *Angewandte Chemie-International Edition* **2020**, *59*, 4684-4690.
(92) He, J. L.; Fang, W. H.; Long, R.; Prezhdo, O. V., Bidentate Lewis Bases Are Preferred for Passivation of Mapbi(3) Surfaces: A Time-Domain Ab Initio Analysis. *Nano Energy* **2021**, *79*, 105491.
(93) Shi, R.; Fang, W. H.; Vasenko, A. S.; Long, R.; Prezhdo, O. V., Efficient Passivation of Dy Center in Ch3nh3pbbr3 by Chlorine: Quantum Molecular Dynamics. *Nano Research* **2022**, *15*, 2112-2122.
(94) Zhao, X.; Fang, W. H.; Long, R.; Prezhdo, O. V., Chemical Passivation of Methylammonium Fragments Eliminates Traps, Extends Charge Lifetimes, and Restores Structural Stability of Ch3nh3pbi3 Perovskite. *Nano Research* **2022**, *15*, 4765-4772.
(95) Jiang, Q.; Zhao, Y.; Zhang, X. W.; Yang, X. L.; Chen, Y.; Chu, Z. M.; Ye, Q. F.; Li, X. X.; Yin, Z. G.; You, J. B., Surface Passivation of Perovskite Film for Efficient Solar Cells. *Nature Photonics* **2019**, *13*, 460-+.

Raw data were generated at the University of Southern California High Performance Computing Center. Derived data supporting the findings of this study are available from the corresponding author on request.